Results in Physics 52 (2023) 106918

Contents lists available at ScienceDirect

Results in Physics

journal homepage: www.elsevier.com/locate/rinp

# Double stranded antiferromagnetic helix as an efficient spin filter

Debjani Das Gupta [a], Santanu K. Maiti [a,*], Laura M. Pérez [b], Judith Helena Ojeda Silva [c,d], David Laroze [e]

[a] Physics and Applied Mathematics Unit, Indian Statistical Institute, 203 Barrackpore Trunk Road, Kolkata 700 108, India
[b] Departamento de Física, FACI, Universidad de Tarapacá, Casilla 7D, Arica 1000000, Chile
[c] Grupo de Física de Materiales, Universidad Pedagógica y Tecnológica de Colombia, 150003 Tunja, Colombia
[d] Laboratorio de Química Teórica y Computacional, Grupo de Investigación Química-Física Molecular y Modelamiento Computacional (QUIMOL), Facultad de Ciencias, Universidad Pedagógica y Tecnológica de Colombia, 150003 Tunja, Boyacá, Colombia
[e] Instituto de Alta Investigación, Universidad de Tarapacá, Casilla 7D, Arica 1000000, Chile

ARTICLE INFO

*Keywords:*
Spin filtration
Double stranded antiferromagnetic helix
Transverse electric field
Tight-binding framework
Beyond nearest-neighbor hopping
Green's function formalism

ABSTRACT

We report a large degree of spin filtration in a double stranded (ds) antiferromagnetic helix (AFH) system. Generally spin channel separation is not possible when a magnetic system possesses a vanishing net magnetization. But we show that a highly polarized spin current can be obtained through the ds AFH when it is subjected to a transverse electric field. Describing the physical system within a tight-binding framework, spin-dependent transport phenomena are studied using the well known Green's function formalism. The effects of chirality (left-handed and right-handed), electric field, electronic hopping (short-range and long-range) in each strand, system temperature, and size of the helix on spin filtration are critically investigated. Two different configurations of magnetic moments in the helix are taken into account, for a more general description. Suitably adjusting the physical parameters, almost cent percent spin polarization can be substantiated and that feature persists even for a broad parameter range. Our analysis may open up a new direction for achieving spin-selective electron transmission and designing of controlled spintronic devices using similar kinds of fascinating helical magnetic systems.

## Introduction

Double stranded helix system has been one of the most promising functional elements since its verification in 2011 by Göhler and co-workers [1]. In their work, they have shown that by depositing self-assembled monolayers of double stranded DNA on a gold substrate, polarized spin current can be obtained from completely unpolarized electrons those are originated from the substrate in presence of light. In the subsequent year, a theoretical proposal came by Guo and Sun [2] where they have shown that a ds DNA can exhibit spin selective electron transmission provided three conditions are satisfied those are (i) molecular chirality, (ii) spin–orbit coupling and (iii) dephasing. Later, a few other attempts have been made along this line to explore different characteristics [3–11]. In all the works available in the literature associated with double stranded helical systems, to the best of our knowledge, spin-dependent scattering occurs due to spin–orbit (SO) coupling [2,4,5,7]. Usually, the SO coupling [12–14] is too weak for molecular systems [15] which in most cases restricts large channel separation between up and down spin electrons, and hence favorable response might not be obtained. It thus opens up the question that whether we can think about any other suitable functional element where spin-dependent scattering strength is quite large than the SO coupled one.

To substantiate this fact, here in our work, we propose a double stranded magnetic helical molecule where the magnetic moments are arranged in such a way that the net magnetization of the system becomes zero. We refer to this system as *double stranded antiferromagnetic helix*. Over the last many years, ferromagnetic materials have been used for spin dependent transport phenomena [16,17]. But there are some major advantages of antiferromagnetic (AF) materials or more specifically we can say magnetic materials with zero net magnetization compared to ferromagnetic ones. For instance, AF materials do not produce any stray fringe field and they are unaffected by external magnetic fields [18,19]. We also do not need to operate an AF system at very low temperatures as the ordering Neél's temperature is reasonably large [20]. Moreover, the operating frequency range of AF is very high (of the order of THz) which helps in designing reading and writing

* Corresponding author.
*E-mail addresses:* debjanidasgupta34@gmail.com (D.D. Gupta), santanu.maiti@isical.ac.in (S.K. Maiti), lperez@uta.cl (L.M. Pérez), judith.ojeda@uptc.edu.co (J.H.O. Silva), dlarozen@uta.cl (D. Laroze).

https://doi.org/10.1016/j.rinp.2023.106918
Received 22 June 2023; Received in revised form 17 August 2023; Accepted 28 August 2023
Available online 1 September 2023

devices and making nano-scale oscillators [21]. Because of these facts, people are now focusing on AF samples which come out as the most promising candidates in the new generation of spintronics [22–26].

In a magnetic sample, spin dependent scattering occurs due to the interaction of itinerant electrons with local magnetic moments placed at different lattice sites. This scattering strength, commonly denoted by the parameter $J$, is considerably large than the SO coupling, and in some cases, it may even reach to few electron-volts [15]. The common perception suggests that a finite mismatch among up and down spin channels does not take place in a magnetic material possessing zero net magnetization, as in such a system the up and down spin Hamiltonians are symmetric to each other. This symmetry can be broken in some ways [27,28], and here in our present work we perform it by applying an electric field along the perpendicular direction of the helix axis. Due to the application of the electric field, site energies of the helix get modified in a cosine form, similar to the diagonal Aubry–André–Harper (AAH) model [29–31], which essentially yields the asymmetry among up and down spin Hamiltonians and brings non-trivial features in helical systems. Moreover, there is a sign reversal in the site energies between the two strands, which gives another interesting behavior in our study. The interplay between the two strands is critically analyzed. To the best of our concern, the chiral induced spin selectivity in a double stranded antiferromagnetic helix has not been reported so far in the extensive literature.

Using a tight-binding (TB) framework, we investigate spin dependent transport phenomena and spin filtration following the well known Green's function formalism [32,33]. Two different handed helices viz, left and right are taken into account, and in each case we consider two types of electron hopping. One is referred to as short-range hopping (SRH) helix and the other is called long-range hopping (LRH) helix [4]. These are very good examples where we can have electron hopping beyond the conventional electron hopping among nearest-neighbor sites. Some of our important aspects and findings are: (i) the electric field is the primary requirement to have spin filtration, (ii) a high degree of spin polarization (close to cent percent) can be obtained even in large bias voltage, (iii) spin selectivity can be monitored by tuning the field strength and its direction, and (iv) for a large temperature range the high degree of spin filtration still persists.

Here, it is relevant to point out that experimentally it is possible to design antiferromagnetic ds helices using various compounds. For instance, P. Yin et al. have shown that antiferromagnetic interaction is present in metal–organic supramolecular network and the strength of this interaction depends on the molecular structure [34]. On the other hand, Z. Gao et al. have studied the magnetic properties of polymer $[Co(dpa)pyz_{0.5}]_n$ (dpa = diphenic acid, pyz = pyrazine) [35]. It also possesses a ds helical structure, and, the magnetic susceptibility data confirms antiferromagnetic interaction in Co ions. In other work, J. Qin et al. have reported that antiferromagnetic interaction remains by changing a nested coaxial helical double column to cationic spiral staircase [36]. Another study has revealed synthesis of self-assembling dicopper(II) helicate with bipyridine ligand [37]. This is also an example of a ds AF helical system. Several other references are also available where antiferromagnetic ordering has been reported in helical geometries [38–41]. With all these suitable evidences, we believe that ds antiferromagnetic helix system can definitely be designed in a suitable laboratory.

The rest part of the paper is arranged as follows. Section "Junction setup, TB Hamiltonian and theoretical formalism" contains the physical description of the ds AFH, its TB Hamiltonian, and the required theoretical framework for the calculations. All the numerical results are presented and carefully analyzed in Section "Numerical results and discussion". Finally, the essential findings of this work are summarized in Section "Closing remarks".

## Junction setup, TB Hamiltonian and theoretical formalism

Here we illustrate the junction setup with the ds AFH, and describe the theoretical framework for the necessary calculations.

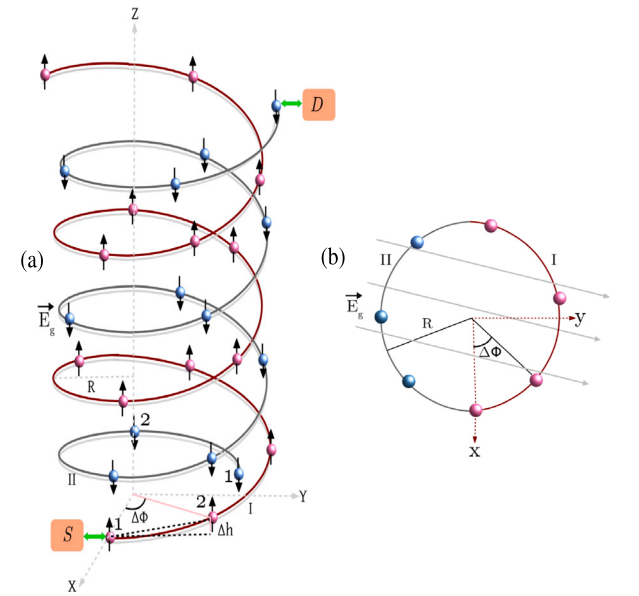


**Fig. 1.** (a) Schematic diagram of a right-handed double stranded antiferromagnetic helix with a specific arrangements of magnetic moments. The helix is sandwiched between source (S) and drain (D) electrodes. In one strand of the helix (strand-I, red curve) all the magnetic moments are aligned along $+Z$ direction, while in the other strand (strand-II, blue curve) all the moments are oriented in the opposite ($-Z$) direction, and thus, the resultant magnetization becomes zero. Three important structural parameters are associated with the helix geometry those are: radius $R$, stacking distance $\Delta h$, and twisted angle $\Delta\phi$. An electric field of strength $E_g$ is applied perpendicular to the helix axis. (b) Projection of the ds helix in XY plane, where two different colored arcs are associated with two different strands. (For interpretation of the references to color in this figure legend, the reader is referred to the web version of this article.)

### Setup and the TB Hamiltonian

Fig. 1 displays the schematic diagram of the junction setup where a double stranded antiferromagnetic helix in presence of a transverse electric field is clamped between source (S) and drain (D). We refer to the two strands as strand-I and strand-II and arrange the magnetic moments in one strand along the $+Z$ direction and in the other strand along the opposite direction, to make the net magnetization of the helix zero. This is one particular configuration of magnetic moments. Other configuration is also taken into account for the completeness of our analysis, and that will be available in the appropriate sub-section. Two fundamental parameters essentially control the helical geometry and regulate the electron hopping. These are, stacking distance $\Delta h$ between neighboring sites and the twisting angle $\Delta\phi$. When $\Delta h$ is reasonably small, electron can hop in all possible sites to make the system a LRH helix, whereas the hopping between the far away sites gets restricted with increasing the stacking distance and the helix maps to a SRH one. In the present work we consider both these helices to have a comprehensive analysis. The contact electrodes are assumed to be one-dimensional, perfect and reflection less.

We describe the junction setup within a tight-binding framework, and explain different terms and factors one by one as follows. The Hamiltonian of the source–helix–drain system can be written as

$$H = H_{mol} + H_{elec} + H_{coup}. \tag{1}$$

There are three terms in the right side of Eq. (1), where the first part is the Hamiltonian of the helical molecule, second term represents the Hamiltonian of the contact electrodes, and the third term denotes the coupling of the helical system with the contact electrodes. For a $N$-site ds AFH ($N/2$ being the total number of magnetic sites in each strand), the TB Hamiltonian reads as

$$H_{mol} = \sum_{j=I,II} \left[ \boldsymbol{c}^{\dagger}_{jk} \left( \boldsymbol{\epsilon}_{jk} - \vec{\boldsymbol{h}}_{jk}.\vec{\boldsymbol{\sigma}} \right) \boldsymbol{c}_{jk} \right.$$

$$+\sum_{k=1}^{N/2-1}\sum_{n=1}^{N/2-k}\left(\boldsymbol{c}_{jk}^{\dagger}\boldsymbol{t}_{jn}\boldsymbol{c}_{jk+n}+h.c.\right)\Big]$$
$$+\sum_{k=1}^{N/2}\left[\boldsymbol{c}_{Ik}^{\dagger}\boldsymbol{\lambda}\boldsymbol{c}_{IIk}+h.c.\right]. \tag{2}$$

The creation operators are written in matrix form as $\boldsymbol{c}_{jk}^{\dagger}=\begin{pmatrix}c_{jk,\uparrow}^{\dagger} & c_{jk,\downarrow}^{\dagger}\end{pmatrix}$ for two spins and its conjugate transpose represents the annihilation operator. $\boldsymbol{\epsilon}_{jk}$ is a $(2\times 2)$ diagonal matrix with identical diagonal elements $\epsilon_{jk}$, which correspond to the site energies at $k$th site of strand $j$ ($j=I,II$) for up and down spin electrons in the absence of magnetic scattering. When an electric field $E_g$ is applied perpendicular to the helix axis, the site energies are modified in a specific form as [2,5]

$$\epsilon_{jk}^{eff}=\epsilon_{jk}-(-1)^{j}eV_g\cos\left(k\Delta\phi-\beta\right). \tag{3}$$

Here $V_g$ is the gate voltage and it is connected to the field through the relation $V_g = E_gR$. $\beta$ represents the angle between the electric field and the positive $X$ axis, and $R$ is the radius (the radius $R$ can be followed clearly from Fig. 1(b)). The spin dependent scattering of itinerant electron occurs due to the term $\vec{\boldsymbol{h}}_{jk}\cdot\vec{\boldsymbol{\sigma}}$ [42,43], where the spin dependent scattering parameter $\vec{h}_{jk}$ depends on the average spin at site $(jk)$ and the coupling strength $J$. In spherical polar co-ordinate system $\vec{h}_{jk}$ is expressed as $(h_{jk},\theta_{jk},\varphi_{jk})$, where $h_{jk}$ is the magnitude and the other two co-ordinates are associated with the polar and azimuthal angles respectively. In our formulation, we assume that all the magnetic moments are of equal strength, and therefore, we set $h_{jk}=h$, without loss of any generality. $\vec{\boldsymbol{\sigma}}$ is the Pauli spin vector, and we assume that $\vec{\boldsymbol{\sigma}}_z$ is diagonal.

The second and third terms of Eq. (2) are associated with the intra- and inter-strand hopping integrals. $\boldsymbol{t}_{jn}$ and $\boldsymbol{\lambda}$ are the intra- and inter-strand hopping matrices, and both of them are diagonal. The intra-strand electron hopping depends on the resultant distance $l_{jn}$ between $k$th and $(k+n)$th sites in the $j$th strand, where [2,4,5]

$$l_{jn}=\sqrt{[2R\sin(n\Delta\phi/2)]^2+(n\Delta h)^2}, \tag{4}$$

and the hopping strength scales as $t_{jn} = t_{j1}\mathrm{e}^{-(l_{jn}-l_{j1})/l_c}$. The factors $l_{j1}$ and $t_{j1}$ denote the nearest-neighbor atomic distance and hopping integral, respectively, and $l_c$ is the decay constant. The inter-strand hopping is considered between the site $k$ of strand-I and site $k$ of strand-II, and the strength is given by the parameter $\lambda$. We can write the two hopping matrices as follows

$$\boldsymbol{t}_{jn}=\begin{pmatrix}t_{jn} & 0\\ 0 & t_{jn}\end{pmatrix}\ \text{and}\ \boldsymbol{\lambda}=\begin{pmatrix}\lambda & 0\\ 0 & \lambda\end{pmatrix}. \tag{5}$$

The contact electrodes source (S) and drain (D), coupled to the ds AFH, are parameterized by the on-site energy $\epsilon_0$ and NNH integral $t_0$. If not specified, the source is coupled to the first site of strand-I and the drain is attached to the end site of strand-II of the helix. Other source–helix–drain configuration is also taken into consideration, to explore the specific role of junction configuration. The coupling strengths of the helix with S and D are denoted by parameters are $\tau_S$ and $\tau_D$, respectively.

*Theoretical framework: Transmission probability, junction current and spin polarization*

We determine the degree of spin filtration by calculating the spin polarization which is the ratio of spin current and charge current, and it is expressed as [44–46]

$$P=\frac{I_{\uparrow}-I_{\downarrow}}{I_{\uparrow}+I_{\downarrow}}\times 100\% \tag{6}$$

where the spin current is $I_S = I_{\uparrow} - I_{\downarrow}$ and the charge current is $I_C = I_{\uparrow} + I_{\downarrow}$. The maximum value of polarization ($P = +100\%$ or $P=-100\%$) is achieved only when one kind of spin flows and other is completely absent, and, the minimum value of $P$ is zero which means that both up and down spin currents propagate equally through the junction.

**Table 1**
Physical parameters of SRH and LRH ds AFHs.

| System | $R$ (nm) | $\Delta h$ (nm) | $\Delta\phi$ (rad) | $l_c$ (nm) |
|---|---|---|---|---|
| SRH | 0.7 | 0.34 | $\pi/5$ | 0.09 |
| LRH | 0.25 | 0.15 | $5\pi/9$ | 0.09 |

The spin dependent current is determined using Landauer–Büttiker formula. Integrating the transmission probability over the allowed energy window across the equilibrium Fermi energy $E_F$ we get the current at finite temperature through the relation [32,33,47]

$$I_{\sigma}=(e/h)\int T_{\sigma}\left(f_S-f_D\right)dE, \tag{7}$$

where $\sigma =\uparrow (\downarrow)$. Here $f_S$ and $f_D$ are the Fermi–Dirac distribution functions of S and D, respectively. The transmission probability $T_{\sigma}$ is evaluated following the Green's function technique. First we calculate the retarded and advanced Green's functions, and they are defined as [32,33]

$$G^R=[G^A]^{\dagger}=\left[E-H-\Sigma_S-\Sigma_D\right]^{-1}. \tag{8}$$

Using $G^R$ and $G^A$, transmission probability is found by taking the trace of the matrix $M_{\sigma}=\Gamma_S G^R\Gamma_D G^A$. The self-energy matrices $\Sigma_{S(D)}$ of the contact electrodes are connected to the coupling energy matrices via the relation $\Gamma_{S(D)}=-2i[\Sigma_{S(D)}]$.

## Numerical results and discussion

Here we present and thoroughly analyze our numerical results of double stranded antiferromagnetic helices under different input conditions. Both the short-range and long-range hopping helices are taken into account, and unless mentioned, we discuss the results of right-handed helix system. The physical parameters that define SRH and LRH ds AFHs are given in Table 1. These values are extensively used in the literature to describe LRH and SRH helical systems [2,4], and accordingly we also choose them. The most common and realistic examples of these two types of helical systems are protein and DNA molecules, respectively [2,4].

The other common parameter values are as follows. We take the spin-dependent scattering parameter $h = 1$. The azimuthal angle $\varphi_{jk}$ is always zero, and the polar angle $\theta_{jk}$ becomes 0 or $\pi$ whether the magnetic moments are aligned along $+Z$ or $-Z$ direction. The intra-strand hopping integrals $t_{I1},t_{II1}$ are fixed to 1 and the inter-strand coupling strength $\lambda$ is also set at 1. The on-site energy $\epsilon_{jk} = 0$. In the side-attached electrodes we take $\epsilon_0 = 0$ and $t_0 = 3$. The coupling strengths are $\tau_S = \tau_D = 1$. All the energies are measured in units of electron-volt. If not specifically stated, the results are worked out setting the temperature at 100 K and considering the right-handed helices with $N = 40$. The effects of helix size and temperature are discussed in separate sub-sections. The rest other parameters those are not common are mentioned in the appropriate parts.

The results are worked our for two distinct configurations of magnetic moments. In one case, the moments in strand-I are aligned along $+Z$ and in strand-II the moments are oriented along $-Z$, as shown schematically in Fig. 1(a). We refer to such a system as type-I ds AFH. Whereas, for the other case, we assume that in each strand the neighboring magnetic moments are aligned along $\pm Z$ directions, which is the most common antiferromagnetic ordering. We call this system as type-II ds AFH. The results of these two types of helices are described below in two-subsections (Sections "Spin-dependent phenomena in type-I ds AFH" and "Spin-dependent phenomena in type-II ds AFH") one by one, to have a complete overview.

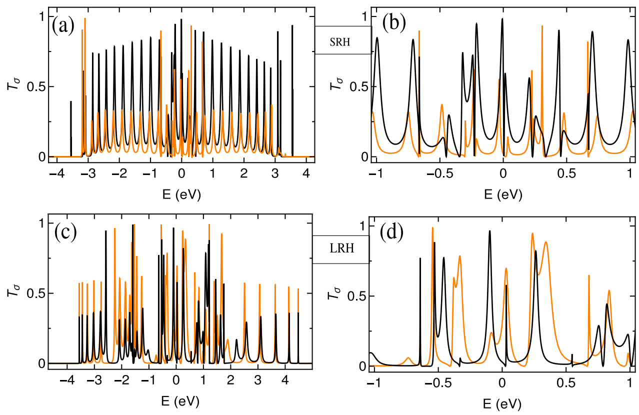


**Fig. 2.** Transmission probabilities of up (black color) and down (orange color) spin electrons, where the first and second rows are associated with the SRH and LRH ds AFHs respectively. In (a) and (c), the transmission spectra are shown in the full allowed energy window, while in (b) and (d) the profiles are shown in a small energy window for a better viewing. Here we choose the gate voltage $V_g = 0.5\,\mathrm{V}$ and $\beta = 0$. (For interpretation of the references to color in this figure legend, the reader is referred to the web version of this article.)

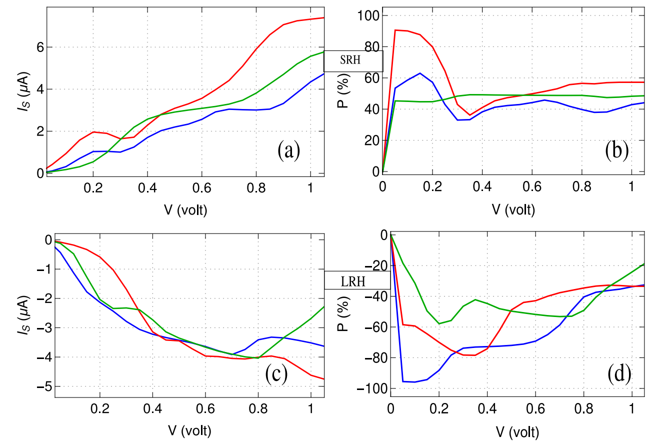


**Fig. 3.** Spin current and spin polarization coefficient for the SRH and LRH ds AFHs at three different Fermi energies, where the blue, red and green curves are for $E_F = -2.2$, 0.5, and 1.6 eV, respectively. The other parameters are same as taken in Fig. 2. (For interpretation of the references to color in this figure legend, the reader is referred to the web version of this article.)

*Spin-dependent phenomena in type-I ds AFH*

*Transmission probability, current and spin polarization*

Let us begin with the transmission-energy characteristics shown in Fig. 2, where the first and second rows correspond to the results of the SRH and LRH helices respectively. In Fig. 2(a) and (c), the transmission curves are plotted in the full energy window. As the number of resonant peaks is reasonably large it is quite difficult to distinguish them appropriately, and therefore, for a clear viewing in Fig. 2(b) and (d), we re-plot the spectra in a small energy window. In each spectrum, two different colored curves are for two different spin cases, and the results are worked out setting the gate voltage $V_g$ at 0.5 V.

Depending on the hopping range, the transmission spectrum gets modified significantly. For the SRH helix, the resonant peaks are almost uniformly spaced. With reducing the hopping range, the spectrum becomes more uniform, and in the NNH case, it is fully symmetric around $E = 0$ (not shown here, as it is well known in the literature). On the other hand, for the LRH helix the peaks are quite irregularly spaced. Towards the bottom of the energy band, the peaks are closely packed, while they are less densely packed in the opposite side of the energy band. This is the generic behavior of the higher order electron hopping. The channel mismatch for the LRH helix is more prominent than the SRH one, and thus, better response is expected for the previous case. In addition, we also see that the transmission-energy spectrum gets splitted into approximately three ranges, which is solely due to the AAH type modulation in site energies. This effect is relatively less reflected in the SRH helix.

From the above analysis it is now clear that through these anti-ferromagnetic helices spin selective currents and spin polarization can be obtained in presence of transverse electric field. To inspect these quantities let us focus on the results given in Fig. 3. Three different Fermi energies are selected and they are represented by three different colored curves. In the first row the results are shown for the SRH helix, while for the LRH helix the results are given in the second row. The system size and the other associated parameters are same as taken in Fig. 2, to have a clear correspondence of the transmission spectra and spin dependent currents. For the SRH case, the spin currents for all the three Fermi energies show positive values, while for the LRH case they are opposite. There is a finite difference in current magnitudes as well. The sign and magnitudes of spin current solely depend on the resonant transmission peaks of up and down spin electrons. When both the spin channels contribute equally no spin polarization is obtained as identical spin currents are there, otherwise a finite spin polarization is available where up and down spin currents are unequal. Inspecting the spectra given in the right column of Fig. 3 it is seen that more favorable response is obtained for the LRH system than the SRH one. On one hand, the degree of spin polarization is high, and on the other hand, it persists over a broad range of bias voltage, which is particularly very essential in the context of experimental realization. Here it is worthy to mention that the choice of the Fermi energy is very crucial. If we choose $E_F$ in a particular region where only one spin channel contributes around the selected energy window associated with the bias voltage, cent percent spin polarization will be obtained, though it is quite difficult to achieve. So, scanning of $E_F$ over the wide region is necessary to have a complete response, and to check where the response is best. These issues are available in the appropriate places of the forthcoming sub-sections.

*Tuning of spin polarization and effects of different physical parameters in type-I ds AFH*

In this sub-section, we concentrate on the possible tuning of spin polarization and critically discuss the effects of different physical parameters associated with the system, by varying them in a broad range, for the sake of completeness of our investigation.

■ **Effects of gate voltage, applied bias and dependence of Fermi energy – Possible tuning**: Fig. 4 shows the density plot of spin polarization co-efficient in two situations. In one case, the variation of $P$ is given in terms of applied bias and the Fermi energy, when the gate voltage is kept constant. While, for the other case, the variation of $P$ is shown as functions of gate voltage (i.e., the electric field) and the direction of the field, when the applied bias and Fermi energy are fixed. The results are quite interesting and important too. For a particular bias voltage, the degree of spin polarization gets modified significantly with the variation of $E_F$ (left panel of Fig. 4). This phenomenon entirely depends on the contributing resonant transmission peaks associated with the up and down spin electrons. Thus the choice of $E_F$ is highly important, and to select the best possible $E_F$ we need to scan over the full Fermi energy window like what is given in Fig. 4(a). The degree of spin filtration efficiency, for any specific $E_F$, gets reduced with increasing the applied bias, since for large $V$, both up and down spin channels contribute to electron transfer, and thus more mixing of electrons occurs which yields lesser value of $P$. Hence, low bias region is much more favorable to have a better response. Similar to Fig. 4(a),

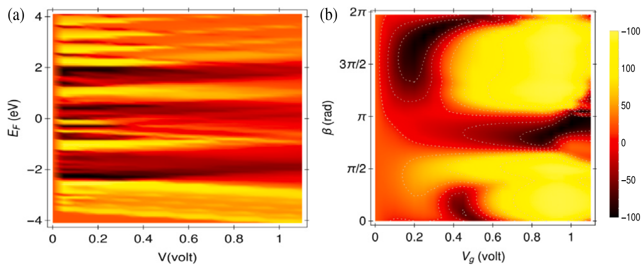

**Fig. 4.** (Color online). Density plot of spin polarization for the LRH helix. (a) Polarization as functions of Fermi energy and bias voltage. Here we take $V_g = 0.5$ V and $\beta = 0$. (b) Polarization as functions of $V_g$ and $\beta$. Here we set $V = 0.2$ V and $E_F = 0.5$ eV.

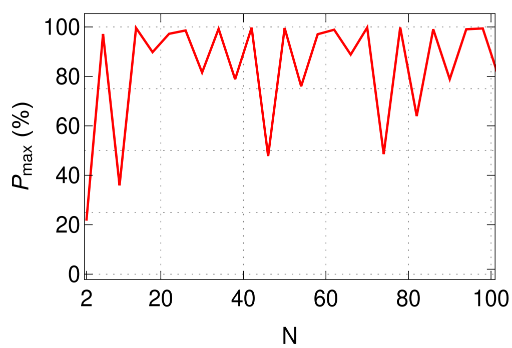

**Fig. 5.** (Color online). Variation of maximum spin polarization $P_{max}$ as a function of system size $N$ for the LRH case. Here we set $V = 0.2$ V, $V_g = 0.75$ V, $\beta = 0$.

(b) suggests that the magnitude and sign of $P$ can be tuned by means of the external electric field and the change of its direction. Almost a complete phase reversal ($+P$ to $-P$, and vice versa) is obtained by adjusting $V_g$ and $\beta$, which might be very interesting in designing of suitable spin-based electronic devices. For lower values of $V_g$, $P$ becomes very small, as expected, since for these cases the mismatch among up and down spin transmission peaks becomes too small. For large values of $V_g$, $P$ becomes very high and reaches close to cent percent. Most importantly, this high degree of spin polarization persists for a reasonably broad parameter windows. For the situation when $P$ reaches to either $+100\%$ or $-100\%$, only up or down spin electrons can propagate through the helix, and thus, it can be stated that the half-metallic state [48] is available in our proposed system.

■ **Dependence of spin polarization on system size and temperature**: The results analyzed so far are worked out for a fixed helix size and fixed system temperature. It is indeed required to check whether any significant change is observed if we vary these parameters. In this sub-section, we discuss these issues one by one. For each helix size, our main aim is to check how much maximum spin polarization is obtained. To inspect it, we compute the maximum of spin polarization (referred to as $P_{max}$) for each $N$, and it is obtained by taking the maximum of spin polarization by varying $E_F$ over the full energy window. The variation of $P_{max}$ with $N$ is shown in Fig. 5, by changing $N$ in a wide range. What we find that, $P_{max}$ oscillates quite irregularly with helix size $N$, and this is entirely due to quantum interference of electronic waves passing through the system. Here we choose a specific set of physical parameters, and selecting any other set, a similar kind of oscillating behavior with $N$ is also observed which we confirm through our detailed numerical calculations. This kind of oscillation in spin polarization has already been reported elsewhere in other related papers [5]. The fact is that, a reasonably high value of $P$ is expected even for moderately large system size. This is an important hint, and might be useful in the context of experimental realization of our proposed prescription.

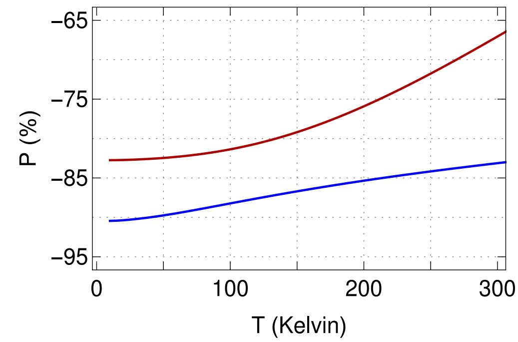

**Fig. 6.** Dependence of spin polarization on temperature at two different Fermi energies for the LRH case, where the blue and dark red curves are for $E_F = -2.2$ and $-0.3$ eV, respectively. The other parameters are: $V = 0.2$ V, $V_g = 0.5$ V, and $\beta = 0$. (For interpretation of the references to color in this figure legend, the reader is referred to the web version of this article.)

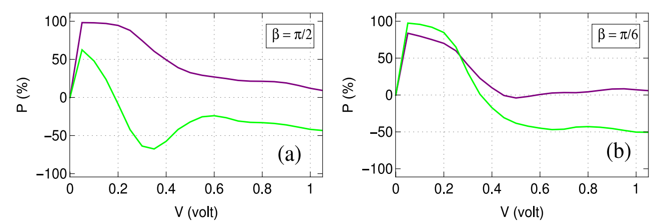

**Fig. 7.** Comparison between right-handed and left-handed LRH ds antiferromagnetic helices. The light green curve is for the left-handed helix and the purple curve is for the right-handed one. We set $V_g = 0.8$ and $E_F = 0.4$ eV. (a) $\beta = \pi/2$ and (b) $\beta = \pi/6$. (For interpretation of the references to color in this figure legend, the reader is referred to the web version of this article.)

The spin polarization is quite less sensitive to temperature (Fig. 6), which is of course highly desirable, as in that case we can have the filtration operation up to a high temperature limit. With increasing temperature, the resonant peaks are broadened, and hence, the probability of getting the contributions from both up and down spin channels increases, which results a reduction of $P$. This effect i.e., the appearance of two spin-dependent energy channels in a particular energy window due to thermal broadening can be reduced, in other way, by choosing small system size such that the average energy level spacing is much higher than the thermal energy. From the curves shown in Fig. 6, it is noticed that high degree of spin polarization still persists over a large temperature limit.

■ **Interplay between right-handed and left-handed ds AFHs**: In the above, all the results are discussed for the right-handed helix only. In this sub-section we concentrate on the effect of handedness, specifically to check how the efficiency gets affected with the alternation of handedness. This effect can be incorporated quite easily into the TB Hamiltonian through a sign reversal of the twisting angle i.e., right-handed to left-handed is obtained through the operation $\Delta\phi \rightarrow -\Delta\phi$ [2, 4]. We need to select the total number of magnetic sites in individual strands in such a way that complete turns are obtained. For our chosen set of physical parameters of LRH helix, we choose 19 sites in each strand which gives two complete turns. Fig. 7 shows the results for the right-handed and left-handed helices at two distinct values of $\beta$. For each $\beta$, there is significant change of $P$ when we alter the handedness of the helix system. This is solely due to the modification of the on-site energies in presence of the external electric field, which directly affects the energy spectra of up and down spin channels, and thus, the spin polarization. So, to have a favorable response, we need to concentrate on the handedness of the helix system as well.

■ **Dependence on position of drain electrode**: Now, we discuss the specific role of source–helix–drain junction configuration on spin-selective transport phenomena. The junction configuration sometimes

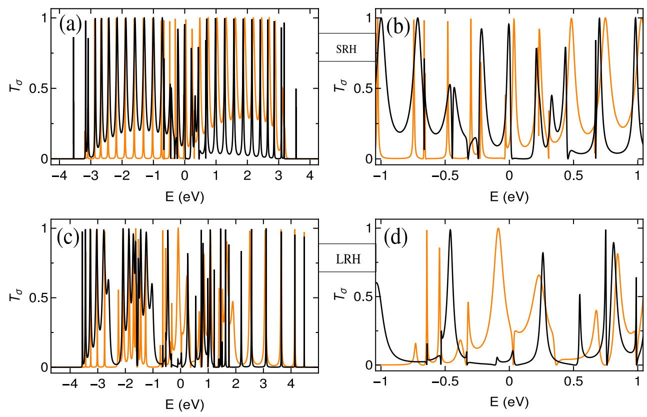


**Fig. 8.** (Color online). Same as Fig. 2, when the drain is coupled to the end site of strand-I. All the physical parameters are unchanged as used in Fig. 2.

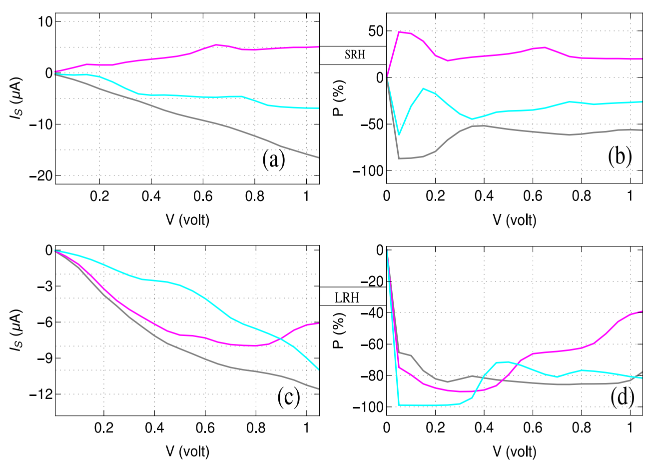


**Fig. 9.** Similar to Fig. 3 where the spin current and spin polarization as a function of bias voltage are shown for the ds antiferromagnetic helices, connecting the source at the first site of strand-I (as earlier) and drain at the end site of strand-I. The magenta, cyan and gray curves are for $E_F = 0$, 0.5 and 1.6 eV, respectively. The rest of other parameters are the same as taken in Fig. 2. (For interpretation of the references to color in this figure legend, the reader is referred to the web version of this article.)

plays an important role, and thus its effect needs to be explored, specifically to check how the spin selectively gets modified with the changing of the drain position. In Fig. 8, we display the results of spin-dependent transmission probabilities both for the SRH and LRH cases, similar to the results presented in Fig. 2, connecting the drain electrode to the end site of the strand-I. The source position remains unchanged. Carefully inspecting the spectra given in Figs. 2 and 8, we can emphasize that the results are quite comparable to each other. No such drastic change is expected. This is somewhat expected as in the helices, electrons can access different possible paths mainly because of the existence of finite connection among the two strands. For the systems where available paths are very less, large change is expected with the variation of the drain position. Such issues have already been discussed earlier in other contemporary works.

Corresponding to the transmission curves given in Fig. 8, in Fig. 9 we show the variation of spin current and spin polarization with bias voltage, at three typical values of Fermi energy. The characteristics features of current and spin polarization are almost similar to what are presented in Fig. 3. The results are sensitive to the choice of the Fermi energy, as expected. Most importantly, a high degree of spin polarization is also obtained for this junction configuration, and like before, LRH helix exhibits favorable response compared to the SRH one.

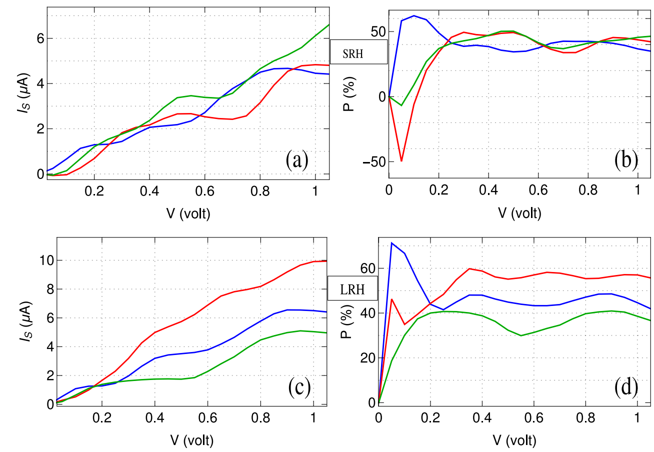


**Fig. 10.** Results in the *absence* of any twisting. Spin current and spin polarization as a function of bias voltage are shown (similar to Fig. 3) for the ds antiferromagnetic ladders ($\Delta\phi = 0$), connecting the source at the first site of strand-I and drain at the end site of strand-II. The three colored curves correspond to the identical Fermi energies as used in Fig. 3. The rest of other parameters are the same as taken in Fig. 2. (For interpretation of the references to color in this figure legend, the reader is referred to the web version of this article.)

■ **Response in the absence of twisting** ($\Delta\phi = 0$): To inspect whether molecular conformation has any significant impact on spin selectivity and to compare the results between the twisted and twist-free systems, here in this sub-section, we discuss the response when there is no twisting i.e., when $\Delta\phi = 0$. Under this situation, the site energies (in the absence of spin-dependent scattering) of all the sites in strand-I become $eV_g$, while for the other strand, the site energies become $-eV_g$ (see Eq. (3)). For the twist-free antiferromagnetic ladders, the results of spin current and spin polarization are shown in Fig. 10. Apart from the twisting, all the other physical parameters and the junction configuration remain unchanged as considered in Fig. 3, to have a direct comparison with the antiferromagnetic ladders in the presence of twisting. Similar to Fig. 3, finite spin currents are obtained both for the SRH and LRH cases (Fig. 10(a) and (c)), but the degree of spin polarization is quite inferior (right column of Fig. 10) compared to what are seen for the SRH and LRH systems when twisting effect is taken into account (right column of Fig. 3). The underlying mechanism is associated with the cosine modulation of site energies for non-zero $\Delta\phi$, which provides a larger mismatch between up and down spin transmission spectra at multiple energy zones. Here it is pertinent to mention that, like our chosen type-I antiferromagnetic ladders where each strand is ferromagnetic (commonly referred to as A-type anti-ferromagnetic system), the electric field induced spin polarization has also been reported in other similar kinds of A-type antiferromagnetic bilayers [24–26].

*Spin-dependent phenomena in type-II ds AFH*

The spin dependent transport phenomena discussed so far are worked out for type-I configuration where the magnetic moments in strand-I are aligned along $+Z$ direction, and for the other strand (strand-II) the moments are aligned along $-Z$ direction. Here, in this sub-section, we analyze the transport phenomena considering a different configuration of magnetic moments, which is schematically shown in Fig. 11. We mention it as type-II configuration. The neighboring magnetic moments in each strand are aligned in the opposite directions, which is the most common arrangement in antiferromagnetic systems (conventionally referred to as G-type antiferromagnetic system). The

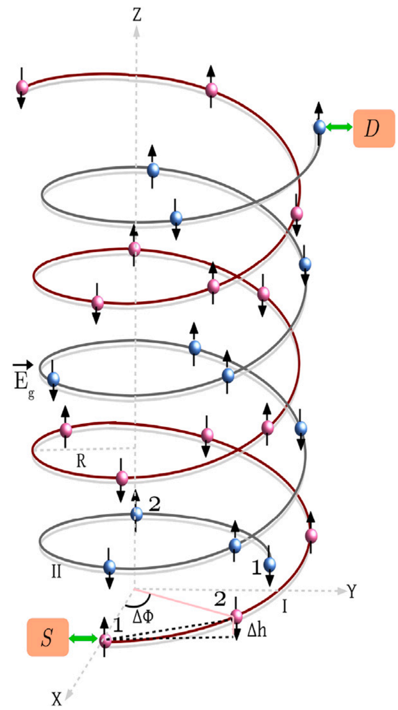

**Fig. 11.** (Color online). Schematic junction setup considering a double stranded antiferromagnetic helix with different arrangement of magnetic moments compared to Fig. 1.

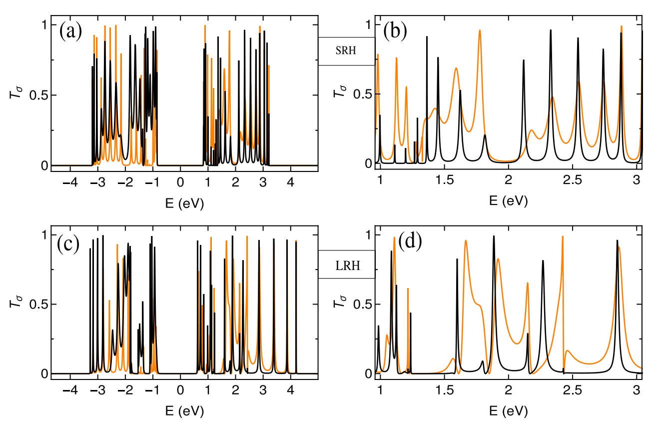

**Fig. 12.** (Color online). Transmission spectra, both in the full and small energy windows, for the junction setup with type-II ds antiferromagnetic helices. The first and second rows are associated with the SRH and LRH cases, respectively. The contact electrodes are coupled to the helices as prescribed in Fig. 11. The physical parameters are same as taken in Fig. 2.

source electrode is coupled to the first site of strand-I and the drain is attached to the end site of strand-II. For the junction setup shown in Fig. 11, we present the results of spin-dependent transmission probabilities as a function of energy in Fig. 12, similar to Figs. 2 and 8. Here it is crucial to point out that, for this G-type antiferromagnetic system where the *net magnetization of each strand is zero*, no separation between up and down spin transmission spectra takes place by the transverse electric field unless the helicity effect is taken into account. It can be understood from the concept of symmetry of the individual strands. As the neighboring magnetic moments in each strand are aligned along $\pm Z$ directions, the Hamiltonians of the two strands are exactly symmetric to each other even in the presence of electric field, when $\Delta\phi = 0$. Thus, for the twist-free case, the up and down spin energy eigenvalues will be identical, and no spin polarization is expected. Once the electric field is applied, the site energies get modulated in the cosine form, as mentioned in Eq. (3). Each strand becomes a correlated disordered one, and most importantly, there is a sign reversal between the site energies in the two strands. All these are directly involved with the helicity of the geometry. Under this situation the symmetry between the two strands gets broken which provides different energy eigenvalues for up and down spin electrons, and hence, a finite mismatch occurs in the transmission spectra, that is clearly seen from the results given in Fig. 12. Both the full and reduced energy windows are taken into account in Fig. 12, like the previous cases. The overall transmission spectrum, be it for up or down spin case, gets modified. A large gap appears around $E = 0$. This is due to the anti-parallel orientation of neighboring magnetic moments. For such an arrangement the effective site energies along each strand become binary alloy type which results a finite gap. The other properties like a finite mismatch among up and down spin transmission curves, dominance of up or down spin transmission probability in a specific energy window compared to the other, and related issues, remain same what are observed for the type-I configuration. So, the general statement is that, even though the net magnetization is zero, a finite separation between up and down spin transmission probabilities might be expected.

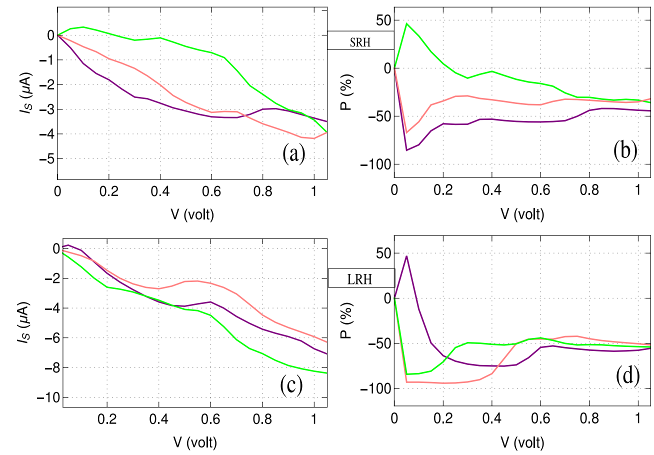

**Fig. 13.** Spin current and spin polarization coefficient for the type-II ds AFHs with the junction configuration used in Fig. 12 at three different Fermi energies, where the purple, green and the pink curves are for $E_F = 1.6$, 2 and 2.5 eV respectively. The other parameters are same as taken in Fig. 2. (For interpretation of the references to color in this figure legend, the reader is referred to the web version of this article.)

Because of this fact, we can expect finite spin current and spin polarization across the type-II helix. The results are given in Fig. 13. It is clearly seen that finite spin current is obtained, and the degree of spin polarization is quite favorable. In some cases, more than 80% spin polarization is achieved. Now, if we compare all the results presented in Figs. 3, 9 and 13, then we can say that the type-I LRH ds AFH with the junction configuration given in Fig. 1 provides the best performance. For this setup, on one hand, the degree of polarization is too high, and on the other hand, this phenomenon persists over a broad range of bias window. Comparing the results of A-type and G-type double-stranded systems it is emphasized that, for the G-type configuration we need to consider both the electric field and the helicity, unlike the A-type configuration where only the electric field is sufficient to have a finite spin polarization.

## Closing remarks

To conclude, in the present work, we report spin filtration operation in a double stranded magnetic helix where the net magnetization is zero. The symmetry between up and down spin Hamiltonians is broken by applying an electric field perpendicular to helix axis. Due to the electric field site energies in each strand becomes correlated in the well known AAH form, and there is a sign reversal for the two strands. The inter- and intra-strand hopping integrals play an important role that is clearly reflected in our investigation. The dependences of different physical parameters associated with the system are thoroughly analyzed. Describing the helix geometry within a tight-binding framework, we compute all the required quantities following the Green's function formalism. What we find is that, a high degree of spin polarization is obtained and that can selectively be monitored by adjusting the field strength and the field direction. Moreover, all the results persist for a wide range of input parameters, which gives us confidence that our proposed prescription can be implemented in a suitable laboratory.

## CRediT authorship contribution statement

**Debjani Das Gupta:** Conceived the project, Performed the numerical calculations, Analyzed the data. **Santanu K. Maiti:** Conceived the project, Analyzed the data. **Laura M. Pérez:** Analyzed the data. **Judith Helena Ojeda Silva:** Performed the numerical calculations. **David Laroze:** Analyzed the data.

## Declaration of competing interest

The authors declare that they have no known competing financial interests or personal relationships that could have appeared to influence the work reported in this paper.

## Data availability

No data was used for the research described in the article

## Acknowledgments

L.M.P. acknowledges financial support from ANID through Convocatoria Nacional Subvención a Instalación en la Academia Convocatoria Año 2021, Grant SA77210040. All authors have read and agreed to the published version of the manuscript.

## References

[1] Göhler B, Hamelbeck V, Markus TZ, Kettner M, Hanne GF, Vager Z, Naaman R, Zacharias H. Spin selectivity in electron transmission through self-assembled monolayers of double-stranded DNA. Science 2011;331:894.
[2] Guo A-M, Sun Q-F. Spin-selective transport of electrons in DNA double helix. Phys Rev Lett 2012;108:218102.
[3] Mishra D, Markus TZ, Naaman R, Kettner M, Göhler B. Spin dependent electron transmission through bacteriorhodopsin embedded in purple membrane. Proc Natl Acad Sci 2013;110:14872.
[4] Guo A-M, Sun Q-F. Spin-dependent electron transport in protein-like single-helical molecules. Proc Natl Acad Sci 2014;111:11658.
[5] Guo A-M, Sun Q-F. Enhanced spin-polarized transport through DNA double helix by gate voltage. Phys Rev B 2012;86:035424.
[6] Rai D, M. Galperin. Electrically driven spin currents in DNA. J Phys Chem C 2013;117:13730–7.
[7] Simchi H, Esmaeilzadeh M, Mazidabadi H. Spin transport and spin polarization properties in double-stranded DNA. J Appl Phys 2013;114:194706.
[8] Zhu W, Guo A-M, Sun Q-F. Electronic transport through tetrahedron-structured DNA-like system. Front Phys 2014;9:774–9.
[9] Simchi H, Esmaeilzadeh M, Mazidabadi H. The effect of a magnetic field on the spin-selective transport in double-stranded DNA. J Appl Phys 2014;115:204701.
[10] Tang H-Z, Sun Q-F, Liu J-J, Zhang Y-T. Majorana zero modes in regular B-form single-stranded DNA proximity-coupled to an s-wave superconductor. Phys Rev B 2019;99:235427.
[11] Pan T-R, Guo A-M, Sun Q-F. Spin-polarized electron transport through helicene molecular junctions. Phys Rev B 2016;94:235448.
[12] Bychkov YA, Rashba EI. Oscillatory effects and the magnetic susceptibility of carriers in inversion layers. J Phys C: Solid State Phys 1984;17:6039.
[13] Dresselhaus G. Spin–orbit coupling effects in zinc blende structures. Phys Rev 1955;100:580.
[14] Premasiri S, Radha SK, Sucharitakul S, Kumar UR, Sankar R, Chou F-C, Chen Y-T, Gao XPA. Tuning rashba spin–orbit coupling in gated multilayer inse. Nano Lett 2018;18:4403.
[15] Su Y-H, Chen S-H, Hu CD, Chang C-R. Competition between spin–orbit interaction and exchange coupling within a honeycomb lattice ribbon. J Phys D: Appl Phys 2016;49:015305.
[16] Tsukagoshi K, Alphenaar B, Ago H. Coherent transport of electron spin in a ferromagnetically contacted carbon nanotube. Nature 1999;401:572.
[17] Kumar S, Kumawat RL, Pathak B. Spin-polarized current in ferromagnetic half-metallic transition- metal iodide nanowires. J Phys Chem C 2019;123:15717.
[18] Baltz V, Manchon A, Tsoi M, Moriyama T, Ono T, Tserkovnyak Y. Antiferromagnetic spintronics. Rev Modern Phys 2018;90:015005.
[19] Jungwirth T, Sinova J, Matri X, Wunderlich J, Felser C. The multiple directions of antiferromagnetic spintronics. Nat Phys 2018;14:200.
[20] Jungfleisch MB, Zhang W, Hoffmann A. Perspectives of antiferromagnetic spintronics. Phys Lett A 2018;382:865.
[21] Artemchuk PY, Sulymenko OR, Louis S, Li J, Khymyn RS, Bankowski E, Meitzler T, Tyberkevych VS, Slavin AN, Prokopenko OV. Terahertz frequency spectrum analysis with a nanoscale antiferromagnetic tunnel junction. J Appl Phys 2020;127:063905.
[22] Kosub T, Kopte M, Hühne R. Purely antiferromagnetic magnetoelectric random access memory. Nature Commun 2017;8:13985.
[23] Němec P, Fiebig M, Kampfrath T, Kimel AV. Antiferromagnetic opto-spintronics. Nat Phys 2018;14:229.
[24] Son Y-W, Cohen ML, Louie SG. Half-metallic graphene nanoribbons. Nature 2006;444:347.
[25] Chen Q, Zheng X, Jiang P, Zhou Y-H, Zhang L, Zeng Z. Electric field induced tunable half-metallicity in an A-type antiferromagnetic bilayer $\mathrm{laBr_2}$. Phys Rev B 2022;106:245423.
[26] Gong S-J, Gong C, Sun Y-Y, Tong W-Y, Duan C-G, Chu J-H, Zhang X. Electrically induced 2D half-metallic antiferromagnets and spin field effect transistors. Proc Natl Acad Sci 2018;115:8511.
[27] Gupta DD, Maiti SK. Can a sample having zero net magnetization produce polarized spin current? J Phys: Condens Matter 2020;32:505803.
[28] Gupta DD, Maiti SK. Spin filtration in an antiferromagnetic ladder. J Magn Magn Mater 2022;546:168813.
[29] Ganeshan S, Sun K, Sarma SD. Topological zero energy modes in gapless commensurate aubry-andré-harper model. Phys Rev Lett 2013;110:180403.
[30] Li X, Sarma SD. Mobility edges in one-dimensional bichromatic incommensurate potentials. Phys Rev B 2017;96:085119.
[31] Roy S, Maiti SK. Tight-binding quantum network with cosine modulations: Electronic localization and delocalization. Eur Phys J B 2019;92:267.
[32] Datta S. Electronic transport in mesoscopic systems. Cambridge: Cambridge University Press; 1997.
[33] Datta S. Quantum transport: Atom to transistor. Cambridge: Cambridge University Press; 2005.
[34] Yin P-X, Zhang J, Li Z-J, Cheng J-K, Qin Y-Y, Zhang L, Yao Y-G. Magnetic investigation of two helical frameworks derived from mixed ligands. Inorganica Chim Acta 2007;360:3525–32.
[35] Gao Z-Q, Gu J-Z, Dou W. Magnetic investigation of a double-helix chain framework based on dinuclear cobalt(II) SBUs. Synth React Inorg Metal-Org Nano-Metal Chem 2009;39:307–11.
[36] Qin J, Jia Y, Li H, Zhao B, Wu D, Zang S, Hou H, Fan Y. Conversion from a heterochiral $[2+2]$ coaxially nested double-helical column to a cationic spiral staircase stimulated by an ionic. Inorg Chem 2014;53:685–7.
[37] Kao H-C, Wang Y-C, Wang W-J. Liquid AnionSyntheses, crystal structure, and magnetic properties of a self-assembling dicopper(II) helicate with novel bipyridine ligand. J Chin Chem Soc 2012;59:934–9.
[38] Clever GH, Reitmeier SJ, Carell T, Schiemann O. Antiferromagnetic coupling of stacked $\mathrm{Cu}^{II}$–Salen complexes in DNA. Angew Chem 2010;122:5047.
[39] Naskar S, Corbella M, Blakec AJ, Chattopadhyay SK. Versatility of 2, 6-diacetylpyridine (dap) hydrazones in generating varied molecular architectures: Synthesis and structural characterization of a binuclear double helical Zn(II) complex and a Mn(II) coordination polymer. Dalton Trans 2007;11:1150.
[40] Daniel M, Vasumathia V. Perturbed soliton excitations in DNA double helix. Phys D: Nonlinear Phenom 2007;231:10.
[41] Malaestean IL, Speldrich M, Baca SG, Ellern A, Schilder H, Kögerler P. Diphenic acid-based cobalt(II) complexes: Trinuclear and double-helical structures. Eur J Inorg Chem 2009;2009:1011.
[42] Shokri AA, Mardaani M, Esfarjani K. Spin filtering and spin diode devices in quantum wire systems. Phys E 2005;27:325.
[43] Shokri AA, Mardaani M. Spin-flip effect on electrical transport in magnetic quantum wire systems. Solid State Commun 2006;137:53.
[44] Patra M, Maiti SK. Externally controlled high degree of spin polarization and spin inversion in a conducting junction: Two new approaches. Sci Rep 2017;7:14313.
[45] Maiti SK. Curvature effect on spin polarization in a three-terminal geometry in presence of rashba spin–orbit interaction. Phys Lett A 2015;379:361.
[46] Gupta DD, Maiti SK. Antiferromagnetic helix as an efficient spin polarizer: Interplay between electric field and higher-order hopping. Phys Rev B 2022;106:125420.
[47] Fisher DS, Lee PA. Relation between conductivity and transmission matrix. Phys Rev B 1981;23:6851.
[48] Khoeini F, Nazari M, Shekarforoush S, Mahdavifar M. Phys E Low Dimens Syst Nanostruct 2020;123:114200.